

Research Paper

Efficient delivery of nucleic acid molecules into skin by combined use of microneedle roller and flexible interdigitated electroporation array

Dong Huang^{1*}, Deyao Zhao^{1*}, Xiaoxia Wang¹, Chunhui Li², Tongren Yang², Lili Du¹, Zewen Wei³, Qiang Cheng¹, Huiqing Cao¹, Zicai Liang¹, Yuanyu Huang², Zhihong Li¹

1. National Key Laboratory of Science and Technology on Micro/Nano Fabrication; Institute of Microelectronics; Institute of Molecular Medicine; Peking University, Beijing 100871, China
2. Advanced Research Institute of Multidisciplinary Science, and School of Life Science, Beijing Institute of Technology, Beijing 100081, China
3. National Center for Nanoscience and Technology, Beijing 100190, China

*These authors contributed equally

#Lead Contact

 Corresponding authors: yhuang@bit.edu.cn (Y. Huang), or zhkli@pku.edu.cn (Zh. Li)

© Ivyspring International Publisher. This is an open access article distributed under the terms of the Creative Commons Attribution (CC BY-NC) license (<https://creativecommons.org/licenses/by-nc/4.0/>). See <http://ivyspring.com/terms> for full terms and conditions.

Received: 2017.10.22; Accepted: 2018.02.07; Published: 2018.03.22

Abstract

Rationale: Delivery of nucleic acid molecules into skin remains a main obstacle for various types of gene therapy or vaccine applications. Here we propose a novel electroporation approach *via* combined use of a microneedle roller and a flexible interdigitated electroporation array (FIEA) for efficient delivery of DNA and siRNA into mouse skin.

Methods: Using micromachining technology, closely spaced gold electrodes were made on a pliable parylene substrate to form a patch-like electroporation array, which enabled close surface contact between the skin and electrodes. Pre-penetration of the skin with a microneedle roller resulted in the formation of microchannels in the skin, which played a role as liquid electrodes in the skin and provided a uniform and deep electric field in the tissue when pulse stimulation was applied by FIEA.

Results: Using this proposed method, gene (RFP) expression and siRNA transfection were successfully achieved in normal mice skin. Anti-SCD1 siRNA electroporated *via* this method mediated significant gene silencing in the skin. Moreover, electroporation assisted by the microneedle roller showed significant advantages over treatment with FIEA alone. This allowed nucleic acid transportation at low voltage, with ideal safety outcomes.

Principal conclusions: Hence, the proposed electroporation approach in this study constitutes a novel way for delivering siRNA and DNA, and even other nucleic acid molecules, to mouse skin *in vivo*, potentially supporting clinical application in the treatment of skin diseases or intradermal/subcutaneous vaccination.

Key words: electroporation, siRNA delivery, gene therapy, flexible interdigitated electroporation array, microneedle roller

Introduction

Gene-based therapies, such as DNA vaccines [1] and tumor vaccines [2], hold great promise to treat cancers, viral infections and inherited diseases [3]. The transdermal delivery of these gene therapeutic agents has become recognized as an important delivery

route, due to the accessibility of skin and because the effect can be easily evaluated clinically and histologically [4]. Furthermore, due to the highly complex and immunogenic functions of a variety of cell types in the skin, such as keratinocytes, fibroblasts

and antigen-presenting cells, the transdermal delivery of gene drugs has shown very promising responses in small and large animal models [5, 6]. Thus gene therapy to the skin has plentiful promising preclinical or clinical applications in the future for treating various skin disorders and systemic diseases [7]. However, skin represents a formidable barrier for transdermal transport of macromolecules mainly due to the stratum corneum [8].

To overcome the skin barrier for transdermal delivery, numerous chemical vehicles, which could enhance the driving force of drug diffusion and/or increase the permeability of the skin, have been developed in the past, such as penetration enhancers, liposomes, micelles, and other vesicles [9-13]. Some of these vesicles showed ideal transportation efficiency [11, 13]. However, they might need to be invasively administered *via* subcutaneous or intradermal injection. In addition, these enhancers could not alter the fundamental properties of the skin, leading to limitations of the amount of drug that can be delivered. Such approaches were incapable of transporting large macromolecules, restricting their use for therapeutic and research applications. Therefore, more direct physical methods that could change the barrier nature of the skin by disrupting the stratum corneum have been explored to enhance transdermal delivery efficiency, which included iontophoresis [14], sonophoresis [15], and electroporation [5, 16-23].

Skin electroporation employs short electrical pulses to change skin permeability by creating an aqueous pathway in the stratum corneum as well as providing an electrical driving force to enhance drug delivery [8]. Due to its high efficiency, versatility, low cost, and biochemical and biological nontoxicity [24, 25], *in vivo* electroporation has been utilized as a promising method to deliver molecules into cells or tissues for clinical applications, such as DNA vaccination [16-19], electrochemotherapy [6, 22, 23] and wound healing [20]. The electrodes used for skin electroporation could be mainly divided into two types, plate (noninvasive) and needle (invasive) electrodes with various configurations [26]. Noninvasive electrodes typically are composed of two plates spaced 1-6 mm apart or other types of contact wires on the skin, such as four plate-electrode (4PE) arrays [27] and wire electrodes on a dish [28]. However, because the electrical resistance of the stratum corneum is orders of magnitude higher than that of hypodermal tissues, and the electrodes are concentrated in the stratum corneum, high voltages are required to generate high electric fields to achieve effective transfection when using such noninvasive electrodes. On the other hand, invasive electrodes

could create an electrical path in the stratum corneum physically and constrain the electric field within the stratum corneum; such devices exhibited more efficient transdermal delivery with lower voltages than noninvasive electrodes. The first hand-assembled dual-needle electrode showed high gene transfer ability [29]. Owing to its convenience of operation and generality, the needle-based electrode has been developed into a commonly used system in laboratories and clinics [30]. Nevertheless, due to the deep needle penetration and relative large distance between needles, needle-based devices might cause severe tissue damage. Additionally, the electric field is also nonuniform in the target tissue, which would negatively affect its performance as well. These issues have limited the clinical application of conventionally fabricated needle-based electroporation devices.

Recently, benefitting from microfabrication technology, pain and muscle stimulation could be avoided by using closely spaced microelectrodes [31]. Utilizing microfabrication technology to shrink the dimensions of the needles and the space between the needles to the range of a few hundred microns, needle matrices [32] and microneedle arrays [33-36] have been developed for direct transdermal drug delivery [37, 38], *in vitro* gene delivery [39, 40] and *in vivo* electroporation [41-43] with remarkably less damage and lower voltages. Furthermore, to enhance the match between the electrode and tissue profile, flexible substrates that can adapt their shape to different tissues have also been explored [42, 44, 45]. A similar strategy as the microneedle-array patches loaded with vesicles can provide fast and efficient drug delivery to the skin [46-49].

Despite all of the advances in these microneedle devices based on micromachining technology, the use of these approaches in humans has received limited attention primarily due to the complexity of device design and high cost of fabrication [31]. To address these challenges, in this paper, we propose a novel strategy with the combined use of a commercial microneedle roller and a flexible interdigitated electroporation array (FIEA) to achieve efficient and low-cost skin electroporation of nucleic acid molecules. The microneedle roller disturbed the stratum corneum and created a series of aqueous paths to deeper tissues, while the flexible planar electroporation array was able to provide close contact with the target surface and produce a homogeneous electric field. Upon penetrating high-resistance stratum corneum, a sufficient hypodermic electric field for efficient electroporation could be established under a low voltage condition and was constrained within the stratum corneum. In addition, the parylene-based pliable electrode and the

microneedle roller were easily available, such that the cost of the method was controlled within an acceptable range, showing high potential in future clinical applications.

Materials and methods

Materials

An RFP (pmRFP-C1) plasmid that encodes red fluorescent protein was used to determine the transfection efficiency of electroporation *in vivo*. The RFP plasmid was purified using a commercial kit (EndoFree Plasmid Maxi Kit, TIANGEN, China). The sequence of Cy5-labelled siRNA (Suzhou Ribo Life Science, Co. Ltd., Kunshan, China) is: sense, 5'-Cy5-CCUUGAGGCAUACUUCAAAAdTdT-3'; anti-sense, 5'-UUUGAAGUAUGCCUCAAGGdTdT-3'. It was stabilized with certain chemical modifications and with a Cy5 fluorophore on the 5' end of the sense strand. siSCD1 targeting stearoyl-CoA desaturase-1 (SCD1) (Catlog: SR3504) was also from Suzhou Ribo Life Science Co. Ltd. It was also chemically modified at certain bases to enhance its stability and avoid potential immune responses. The sequences of PCR primer sets of SCD1 were as follows: forward primer, 5'-TGGTGAACAGTGCCGCGCAT-3'; reverse primer, 5'-ACTCAGAAGCCCAAAGCTCAGCTAC-3'. In addition, the sequences of primer sets of GAPDH were as follows: forward primer, 5'-AACTTTGGCATTGTGGAAGGGCTC-3'; reverse primer, 5'-TGGAAGAGTGGGAGTTGCTGTTGA-3'. All these primers were purchased from CapitalBio Corporation (Beijing, China). SCD1 antibody was from Abcam China (Shanghai, China). GAPDH antibody was from Proteintech Group (Wuhan, China).

Reverse transcription kit and real-time PCR kit were from Promega Corporation (Fitchburg, Wisconsin, USA) and Beijing ComWin Biotech Co.,Ltd. (Beijing, China), respectively. Depilatory cream (Veet®) was purchased online from JingDong Website. RNAlater® and RNazol® were from Sigma-Aldrich (St. Louis, MO, USA). Optimal cutting temperature (OCT) compound was purchased from Sakura Finetek USA, Inc. (Torrance, CA90501, USA). DAPI (4',6-diamidino-2-phenylindole, for staining nuclei) and fluorescein isothiocyanate-labelled phalloidin (for staining F actin) were purchased from Zhongshan Goldenbridge Biotechnology Co. Ltd., Beijing, China and Sigam-Aldrich, USA, respectively.

Commercial microneedle rollers are widely used in transdermal pharmaceutical delivery and medical cosmetology. We chose DRS Dermaroller System 600 series (Derma Roller System, Ltd., Germany), with a high-density microneedle array, to perform the studies in this work. There were 10 rows of needles on

the head with 60 units per row, as shown in **Figure S1**. DRS Dermaroller System 600 could provide several models with different needle lengths for treatment of different areas of the body depending on the thickness of the target skin. Here, 0.5 mm long, 1.0 mm long and 1.5 mm long models were used in these experiments.

Fabrication of flexible interdigitated electroporation array (FIEA)

The flexible electrode patch was designed as planar rectangular interdigital microelectrodes that could produce a uniform electric field in the target tissues [44]. Considering bio-compatibility and flexibility, gold and Parylene C were chosen as the electrode and substrate materials, respectively. Additionally, good transmission of light could also offer real-time monitoring throughout the whole electroporation process. The flexible electroporation patch was manufactured with microfabrication technology based on MEMS (micro-electromechanical system) processes. The process is illustrated in **Figure S2**. Firstly, about 10 μm Parylene C was deposited on the thermal silicon oxide layer, approximately 3000 \AA , with a PDS2010 system (Specialty Coating System, USA). Then, 300 \AA chromium and 1000 \AA gold were sputtered on Parylene as adhesion layer and seed layer, respectively. After that, 12 μm AZ4620 photoresist was patterned as a mold on the wafer using spin-coating and photolithography processes. In order to make sure that the electrode could withstand relatively high voltage, electroplated Au with a thickness of 10 μm was employed as the electrode material. Lastly, photoresist, seed layer and silicon oxide were removed to obtain the flexible electrode.

Finite element analysis

We established a finite element analysis model in COMSOL 5.2 (COMSOL Inc., Sweden) to estimate the field distribution. The model utilized the Electric Currents module to fully capture the electric field contribution within the computing domain. The main parameters (electric conductivity) of the materials used in the simulation were: 0.1 S/m for tissue, 3.5 S/m for conductive buffer and 4.5 MS/m for gold [50]. The boundary of two electrodes was defined as voltage source and ground. The other boundaries were set as electric insulation except for two vertical boundaries, which were defined as periodic boundary to simulate the actual situation. A hyperfine triangle mesh approach with more than 5.6×10^5 elements was used to ensure accurate results.

Animals

Male C57BL/6 mice (age 6–8 weeks) for *in vivo* electroporation were purchased from Vital River

Laboratories (Beijing, China). Animals were maintained in Peking University Laboratory Animal Center, which is an AAALAC-accredited and specific pathogen-free (SPF) experimental animal facility. All of the experimental animals in our study were treated in accordance with protocols approved by the Institutional Animal Care and Use Committee of Peking University.

Preparation of fluorescent frozen sections

To verify the existence and duration time of liquid conductive microchannels in the skin by rolling with a microneedle roller, fluorescent cryosections were prepared and observed with a confocal microscope. In brief, 10 μ L Cy5-labeled siRNA was smeared on pre-depilated mouse thigh skin, followed by rolling with a 1.5 mm long microneedle roller immediately. In addition to the untreated control group, mouse skin daubed with the same amount of Cy5-siRNA and rinsed with water at 10 min after daubing, but without rolling treatment, was included as a control. Animals were sacrificed by cervical dislocation at indicated time points (5 min, 10 min, 30 min and 60 min for mice with rolling treatment; 0 min for control animals). Tissue samples (skin together with its adherent muscle) were collected and placed on Omnisette tissue cassettes, embedded in OCT, and frozen in a pre-chilled Dewar flask containing a liquid nitrogen/dry ice slurry for \sim 1 min until the OCT turned white and opaque. Subsequently, the specimens were cut into 10 μ m sections on a cryostat. Each section was picked up on a glass slide, stained by DAPI for viewing the nuclei and by FITC-labelled phalloidin to visualize F actin in order to display the rough outline of the cell. Finally, cryosections were examined under a confocal microscope.

For cryosection observation of electroporated Cy5-labelled siRNA in skin, 10 μ L Cy5-labeled siRNA was also daubed on pre-depilated mouse thigh skin, followed by rolling with 0.5 mm long microneedle roller. Electroporation was performed with FIEA at 70 V one minute after rolling. Then cryosections were prepared and observed with the above-mentioned protocol.

Electroporation of RFP or Cy5-labelled siRNA for *in vivo* imaging

To evaluate the nucleic acid transfection efficiency with the proposed electroporation protocol, red fluorescent protein (RFP) expression plasmid was selected in this assay. Mouse hair around its right thigh was depilated with depilatory cream (Veet®) one day before electroporation. First, the conductive liquid buffer (\sim 100 μ L) was dropped on the surface of the testing skin, and the microneedle roller (DRS

DermaRoller System 600, Derma Roller System, Ltd., Germany) was rolled on the skin lightly 10 times vertically and horizontally. After adding 10 μ L RFP plasmid (1 μ g/ μ L) onto the skin of interest of treated mice, FIEA was covered on the skin, and 10 electric pulses, with a pulse duration of 10 ms and a 1 s interval between each pulse, provided by Electro Square Porator™ ECM 830 (BTX, San Diego, CA, USA), were applied for electroporation. No electric pulses were applied for the control mice. Finally, the mice were carefully maintained until examination of RFP expression with an *in vivo* imaging system. Meanwhile, safety assessment was performed for two weeks according to the 'Guidance for Industry-Single Dose Acute Toxicity Testing for Pharmaceuticals' [51], to determine if there was any skin damage or physical dysfunction.

For siRNA electroporation, 10 μ L Cy5-labelled siRNA (1 μ g/ μ L) was painted on the skin of interest of treated mice. Other procedures were the same for RFP electroporation, except one mouse was sacrificed at 6 h post treatment for each group of mice to examine Cy5-siRNA signal in isolated skins.

In vivo fluorescence imaging

To evaluate the electroporation efficacy of the proposed schedule, fluorescence imaging with an *in vivo* imaging system (Carestream In-Vivo Imaging System FX Pro, Carestream Health, USA) was performed. Twenty-four and forty-eight hours post electroporation, RFP expression in the skin was examined. 550 nm excitation and 600 nm emission filters were chosen for the experiment. According to the manufacturer's specification, the bandpasses of such excitation and emission filters are 20 nm and 60 nm (wide angle), respectively, suggesting the excitation and emission spectra are 540-560 nm and 570-630 nm, respectively. Other detailed exposure conditions were as follows: exposure time, 60.0 s (2 min for the assay of **Figure S5**); x-binning, 2 \times binning; y-binning, 2 \times binning; f-stop, 2.50; FOV, 180 mm; focal plane, 13.0 mm. The mice were anesthetized with a mixed gas of isoflurane and oxygen before and during imaging.

For detection of the fluorescence signal of Cy5-labelled siRNA, images were acquired at 6 and 24 h post electroporation. Here, the 630 nm excitation and 700 nm emission filters, with the excitation and emission spectra of 620-640 nm and 670-730nm, respectively, were chosen for the experiment. The other imaging conditions were the same as for RFP imaging.

Finally, the signal intensity of RFP or Cy5 was quantified using a molecular imaging software package (Carestream Health, USA). Presented

fluorescence data of both RFP and Cy5 are the average of four (or three) independent assays. All data are shown as the mean \pm SEM.

Real-time quantitative PCR

Real-time quantitative PCR was used to investigate whether siRNA electroporated by the proposed method could mediate gene silencing in the skin. Anti-SCD1 siRNA (siSCD1) was used in this assay. Normal male C57BL/6 mice, weighing \sim 20 g, were randomly divided into five groups (6 mice per group), followed by administration of the following treatments: (1) electroporation assisted by roller but without administration of siRNA, (2) smearing siRNA on the skin and rolled with the roller but without electroporation, (3) electroporation of siSCD1 without rolling, (4) electroporation of siSCD1 assisted by 0.5 mm long roller, (5) electroporation of siSCD1 assisted by 1.5 mm long roller. The electric pulse was given at 70 V (10 pulses, 10 ms duration, 1 s interval). siRNA was dosed at 10 μ g per mouse (1 μ g/ μ L, \sim 0.5 mg/kg).

Skin samples were collected at 48 h post electroporation, and subjected to RNAlater[®] (Sigma-Aldrich). Subsequently, tissues were homogenized with a homogenator, followed by addition of RNAzol (Vigorous Biotechnology Beijing Co., Ltd., Beijing, China) and extraction of total RNA according to a standard protocol. cDNA was prepared by incubating the reaction mixture (4 μ L of MgCl₂ (500 mM), 2 μ L of reverse transcription buffer (10 \times), 2 μ L of dNTP mixture (10 mM), 0.5 μ L of recombinant RNasin, 0.5 μ L of AMV, 1 μ L of Oligo d(T) and 10 μ L pf total RNA) at 42 °C for 15 min, 95 °C for 5 min and 4 °C for 5 min. Then a real-time PCR reaction system (10 μ L of reaction mix, 1 μ L of forward primer (5 μ M), 1 μ L of reverse primer (5 μ M), 1 μ L of cDNA template and 7 μ L of ddH₂O) was prepared and first hot-started for 10 min at 95 °C before 40 cycles of 30 s at 95 °C, 30 s at 60 °C and 30 s at 72 °C. After the melting procedure was completed, samples were stored at 4 °C. Expression levels of SCD1 were analyzed by the Ct (cycle threshold) values with a standard protocol. GAPDH (glyceraldehyde 3-phosphate dehydrogenase) was selected as the reference gene, and its PCR reaction condition was the same as the parameter settings for SCD1.

Western blot

Western blot was also used to evaluate gene silencing efficiency in the skin. Except for the addition of an untreated control group, the other treatments were the same as those treatments in the RT-PCR assay. Skin samples were also collected at 48 h

post-treatment, and homogenized with a homogenizer.

Then, total proteins were extracted by cell lysis buffer (50 mM Tris HCl, pH 7.4, 150 mM NaCl, 1 mM EDTA, 1% TRITON X-100), and 80 μ g of protein from each lysate was separated by SDS-PAGE and transferred onto a nitrocellulose filter membrane (Millipore). The membrane was blocked and incubated at 4 °C overnight with primary antibodies (antibody to SCD-1 (ABcam, UK), antibody to GAPDH (Proteintech, Wuhan, China)). Then the membrane was washed and incubated at room temperature for 1.5 h with secondary antibodies (Zhongshan Goldenbridge Biotechnology Co. Ltd., Beijing, China). Finally, the membranes were exposed using Bio-Rad Universal Hood II (Bio-Rad, Bossier City, LA).

Acute toxicity assessment

To evaluate the potential damages resulting from the proposed electroporation protocol, standard acute toxicity assessment procedures were performed for both studies of RFP and Cy5-labelled siRNA electroporation according to the 'Guidance for Industry-Single Dose Acute Toxicity Testing for Pharmaceuticals' issued by the China Food and Drug Administration (CFDA) [51]. Briefly, after electroporation, all animals were carefully fed for two weeks. Clinical symptoms, including animal appearance, behavior, eating, drinking, response to stimulation, excretion, as well as skin appearance and muscle function at the electroporation position, were recorded during the whole process. Photo images were collected at indicated time points (e.g., five days post electroporation).

Histopathologic analysis

To further evaluate the safety of the proposed electroporation method, histopathologic assessment was also performed. Male C57BL/6 mice (aged 6–8 weeks) were divided into four groups with 2 animals per group. Thigh hair was depilated one day before the mice received the following treatments: (1) without any treatment; (2) rolled with 1.5 mm long roller, but without electroporation; (3) electroporated at 70 V with FIEA, but without rolling; (4) rolled with roller followed by electroporating at 70 V with FIEA. Animals were sacrificed by cervical dislocation and tissue samples (skins with their adherent subcutaneous muscle) were collected on days 1, 3, 6 and 10 post treatment. Then histopathologic sections were prepared with a standard protocol and H&E staining was carried out. Finally, sections were observed and analyzed with an inverted microscope (Olympus X71, Olympus, Tokyo, Japan).

Statistical analysis

Data are expressed as the mean \pm SEM. Statistical analyses were performed using two-tailed Student's t-test to measure statistical differences among groups. Data with $p < 0.05$ were considered to be statistically significant.

Results and discussion

Design of skin electroporation method

The main process of the proposed minimally invasive *in vivo* electroporation method applied on the thigh skin of mice is illustrated in **Figure 1**. Before the electroporation, the target mice were preprocessed. The mice were anesthetized by intraperitoneal injection with chloral hydrate (4% w/v) at a dose of 10 mL/g, and carefully depilated on the right leg with depilatory cream (Veet®) one day before electroporation to facilitate observation.

Firstly, the conductive liquid buffer was coated on the surface of the skin, and the microneedle roller (DRS Dermaroller System 600, Derma Roller System, Ltd., Germany; **Figure S1**) was rolled on the skin lightly 10 times vertically and horizontally. Conductive buffer can be replaced with nucleic acid solution since they all are conductive solutions. These delicate needles gently and painlessly pierced the skin, creating a series of microchannels (pore size was about 125 μm and 180 μm for the 0.5 mm long and 1.5 mm long microneedle rollers, respectively [52]) in the skin as shown in **Figure 1**. These microchannels would be filled by the conductive buffer immediately, forming a conductive path. This step could enhance skin permeability and reduce the tissue electric resistance because the high-resistance stratum corneum was penetrated. Then, the target drug was smeared on the treated area on the skin. After that, the flexible interdigitated electroporation array (FIEA; **Figure S2**) was tightly attached on the skin to match the skin profile, followed by application of electric pulses. When electroporating, the buffer in the

microchannels, forming liquid conductive paths, could play the role of inner electrodes to generate sufficient hypodermic electric field to accomplish highly efficient electroporation, even under a low applied voltage. Finally, the mice were cultivated for further examinations.

Electric field analysis

Here, we set up simplified models to analyze the electric field contribution under treatment with FIEA only or treatment with the combined use of a 0.5 mm long microneedle roller and FIEA, to illustrate the enhancement in skin electroporation by our method. It was reported that the diameter of the pores caused by the 0.5 mm microneedle roller are approximately 125 μm [52]. Therefore, we assumed that the geometric shape of the microchannel was a cone 125 μm in diameter and 500 μm in height. Additionally, the mismatch between the conductive microchannel and the rectangle interdigital microelectrode was ignored to simplify the model. We set the electric conductivity of the golden electrode, conductive buffer and tissue as 4.5 MS/m, 3.5 S/m and 0.1 S/m, respectively [50]. The details of the model domain boundaries are described in **Figure S3**.

The result of the electric field simulation (COMSOL 5.2, COMSOL Inc., Sweden) is shown in **Figure 2**. It could be estimated that our method was able to generate a more homogeneous and stronger field beneath the skin, compared with using FIEA only at the same voltage. With the assistance of the conductive microchannels (**Figure 2A**), the light blue area (400 V/cm to 600 V/cm), which was suitable for electroporation, was much larger than that without rolling with the microneedle roller (**Figure 2B**). It is worth mentioning that, to simplify the model as much as possible, the thin stratum corneum layer was also ignored, which has high resistance. In other words, the electric field would be much weaker in the actual situation for the sample without rolling treatment.

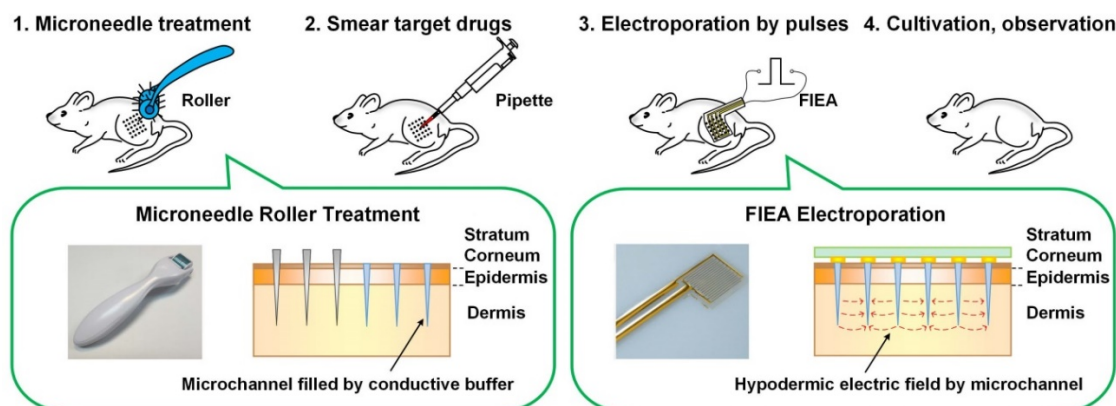


Figure 1. The main processes of the proposed *in vivo* electroporation strategy.

The curves in **Figure 2C** represent the electric field strengths at the centerlines in the middle of adjacent electrodes. When 50 V was applied, the electric field generated with assistance of the conductive path was much stronger than FIEA only, but slightly lower than a metal material microneedle with the same geometric dimension. The conductivity of the metal microneedle is a few orders of magnitude larger than that of liquid buffer. However, microfabrication of microneedles with this size is challenging and costly. Therefore, with assistance from the microneedle roller, a satisfactory electric field could be achieved with a lower voltage and lower cost.

Characteristics of the method

In contrast to previous needle-based *in vivo* electroporation techniques, the proposed approach was found to have the following prominent characteristics: (i) The cost was low. We previously developed another pliable patch integrated electrode

[44] and microneedle array [33] to enhance the performance of *in vivo* electroporation. However, the high cost and high complexity of the microfabrication process restricted its practical application. In contrast, the proposed technique provides a viable alternative in that both the microneedle roller and the flexible electrode patch are reusable, and the fabrication proved that the cost could be significantly reduced by mass production. (ii) The pliable substrate could match the surface profile of the skin. (iii) Damage to the target skin induced by the proposed approach was less than for other needle-based methods, as the invasiveness of these other methods is more severe. Visual examination of skin appearance under a microscope before and after 0.5 mm long microneedle roller treatment is shown in **Figure S4**. In the field-of-view, the skin damage was very slight after rolling. No significant difference was recorded under the microscope. (iv) The dimension of the target region could be easily enlarged, supporting electrochemotherapy or other drug delivery over a large area.

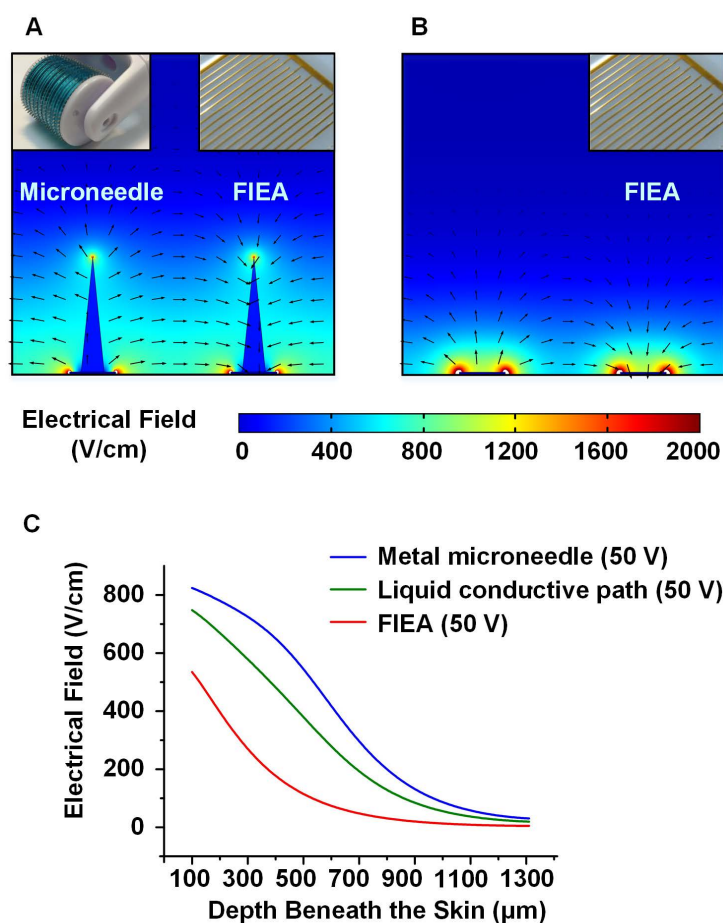


Figure 2. The simplified model and analysis of the electric field. **(A-B)** The electric field generated with and without microneedle treatment, from which we could estimate the distribution of the subcutaneous electric field under different conditions. **(C)** Correlation curves between the electric field strength and the depth beneath the skin (100-1300 μm). Compared with the metal microneedle and the planar electrode, the liquid conductive microchannel could generate a satisfactory electrical field beneath the skin with a lower voltage and lower cost.

Establishment of liquid conductive microchannels in skin

Due to the assistance of the microneedle, liquid conductive paths can be constructed in skin, which will facilitate *in vivo* electroporation with low-voltage electric pulses. To confirm the existence of liquid conductive microchannels, and to evaluate the duration time of these channels, we employed Cy5-labelled siRNA as a tracer. Ten micrograms of Cy5-siRNA (1 $\mu\text{g}/\mu\text{L}$) was first smeared on pre-depilated mouse thigh skin, followed by rolling with a 1.5 mm long microneedle roller. Mice were sacrificed at indicated time points (5 min, 10 min, 30 min, and 60 min) post treatment, and cryosections were prepared and analyzed with a confocal microscope. It was observed that a discontinuity existed on the skin, and the Cy5 signal localized in those holes in the skin (**Figure 3A**, white arrowhead). This demonstrated that the liquid conductive microchannels were successfully established with the proposed microneedle roller. The pore sizes ranged between 150 and 220 μm , which is consistent with the reported data ($\sim 170 \mu\text{m}$) [52]. Moreover, the channels could exist for more than 60 min, as the holes could be observed at all time points (**Figure 3A**), which is also in line with the reported data [52].

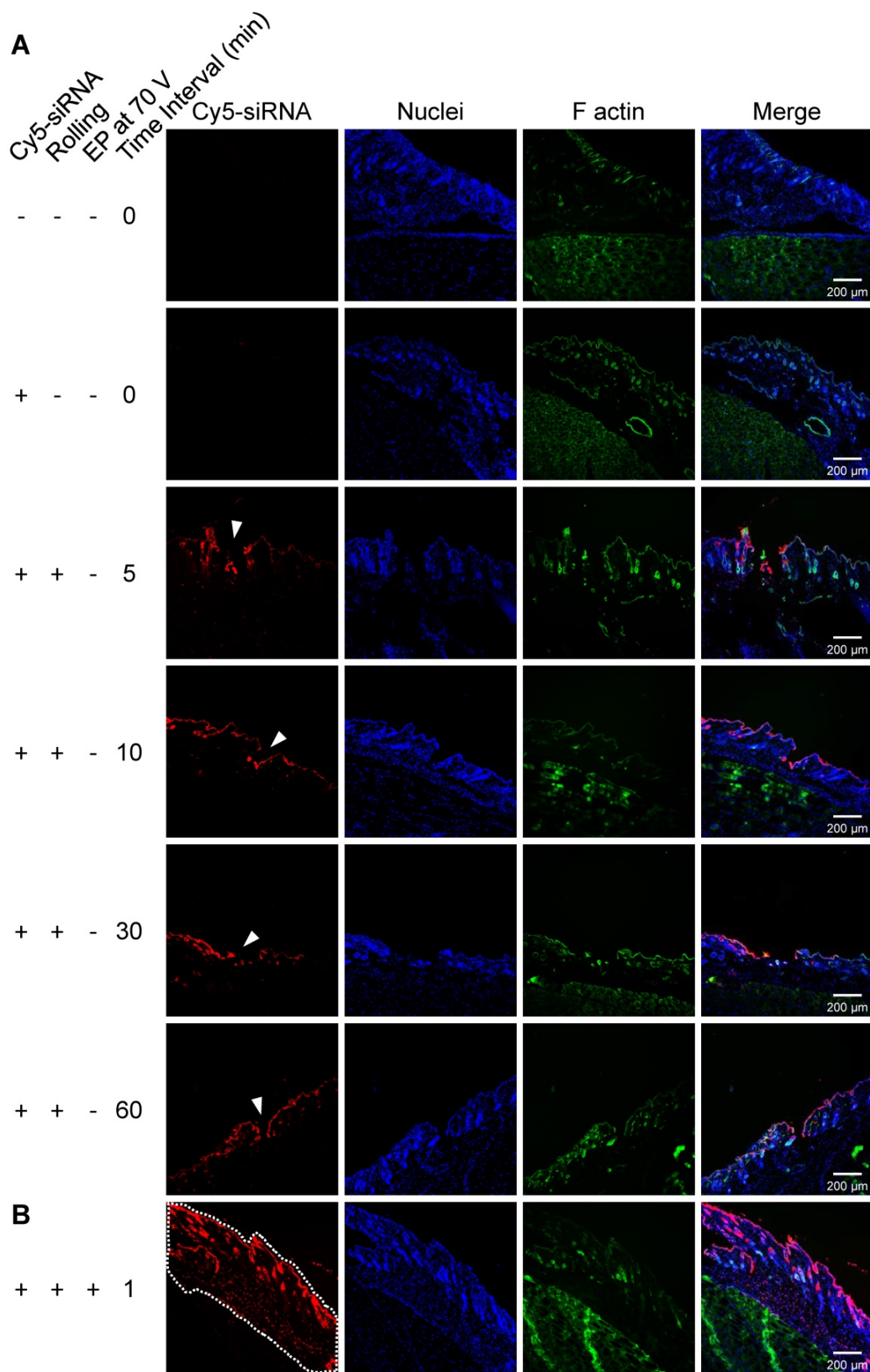


Figure 3. Confocal fluorescence images of the skin cyrosections. Red, Cy5-labelled siRNAs; blue, nuclei stained by DAPI; green, F-actin stained by FITC-labeled phalloidin. **(A)** Fluorescence image of the microchannels (white arrowhead) generated by rolling with a 1.5 mm long microneedle roller. The upper two panels of images are controls without Cy5 signal on the skin, and the lower panels are samples collected at indicated time points (5 min, 10 min, 30 min, and 60 min) post rolling treatment. The fluorophore (Cy5-labeled siRNA) existed in the microchannels, suggesting that the conductive solution entered the microchannels smoothly, forming liquid conductive paths in the skin. **(B)** Cy5-siRNA electroporation with the proposed method. To verify the depth of siRNA delivery using the proposed electroporation method, a 0.5 mm long microneedle roller, the shortest one we used in this study, was applied to perform this assay. Uniform fluorescence signal was recorded in whole full-thickness skin, as the white dotted line indicates.

Gene electroporation and expression in skin

Transfer of genes or nucleic acid molecules to the skin is a promising strategy for the treatment of local skin disorders and also for systemic diseases [53, 54]. The skin consists of epidermal dendritic cells known as Langerhans cells, which can produce and release polypeptides into the circulation. Additionally, the skin is an attractive target for gene transfer owing to its large size and accessibility. To investigate transdermal nucleic acid delivery by the proposed electroporation method, we investigated the transfection of red fluorescent protein (RFP) plasmid to the skin of mouse legs using the protocol described in detail in the section 'Design of skin electroporation method'. Here, we employed a RFP-expressing plasmid to conduct this assay since the background autofluorescence of the mice under RFP excitation/emission spectrum is not strong. Therefore, RFP signal could be easily distinguished from the background signal. Moreover, compared with shorter wavelength fluorophores, near-infrared (NIR) fluorophores (e.g., RFP) are superior in their tissue-penetration capacity [55]. The mice were divided into 6 groups. Each group received a different treatment: (G1) without any treatment as negative control; (G2) electroporation with plate electrode at 100 V; (G3) electroporation with FIEA at 50 V without rolling; (G4) electroporation with FIEA at 50 V with rolling; (G5) electroporation with FIEA at 70 V without rolling; (G6) electroporation with FIEA at 70 V with rolling. The plasmid expressions were examined at 24 h and 48 h after electroporation (exposure time, 1 min). Data showed that the negative control group (G1) showed no fluorescence on the leg, which meant no RFP was expressed (Figure 4A-B). The mice treated by the plate electrode at 100 V, the positive control, showed successful transfection of RFP, but the level of expression was relatively low. By contrast, application of FIEA (G3, G5) could significantly enhance the gene transfer efficiency even at a lower voltage. The mice from G3 showed stronger fluorescence than those of G2, and the areas of skin expressing RFP were also larger than those of G2. On the other hand, with the assistance of the microneedle roller, plasmid electroporation into the mouse skin in G4 and G6 showed better performance than G3 and G5, respectively (Figure 4A-B). This indicated that the microchannels, generated by the microneedle roller and filled with the conductive liquid buffer, played a role as inner electrodes, which remarkably enhanced the transdermal gene transfection efficiency.

The mean fluorescence intensity (MFI) of these treated groups was further analyzed quantitatively, as shown in the histograms of Figure 4D. The MFI of G4 (using FIEA at 50 V) was increased 5-6-fold compared

to the skin with plate electrodes at 100 V (G2), which indicated that our technique could provide an access to highly efficient transdermal electroporation under low voltage. Low voltage will theoretically induce less tissue damage. These data demonstrated that the proposed approach could remarkably enhance the skin electroporation performance even at low voltage by creating a series of microchannels in the stratum corneum as a conductive path.

Influence of time interval on electroporation efficiency in skin

The time interval between microneedle and FIEA treatment should be considered as an important potential influencing factor for the suggested electroporation protocol. According to a previous report [52], the pore size might decrease from 180 μm to 75 μm 2 h after treatment with a 1.5 mm long microneedle roller. The recovery rate reached over 90% 6 h after treatment. Hence, the microchannels could exist for several hours, which was also consistent with our own data (Figure 3A). For the protocol employed in the above-mentioned study, electroporation with FIEA was applied within one minute after rolling.

Here, RFP expression plasmid was also daubed on the skin, and rolled with the 1.5 mm long roller. However, electroporation was given at different time points (1 min, 5 min, 10 min, 15 min and 30 min) after rolling treatment. Fluorescence imaging was performed at 48 h and 72 h post treatment (exposure time, 2 min). It was observed that RFP was successfully expressed in all groups of mice receiving electroporation (Figure S5). More importantly, there was no significant difference among the mice receiving electroporation at different time points (Figure S5), suggesting that a time interval within 30 min was not a dominant issue for the proposed electroporation method. Although a longer time interval was not tested in this assay, a time interval of 30 min is long enough for normal operation in future studies.

Gene electroporation and expression in myocytes

In order to verify that the suggested approach could provide access to penetrate the high-resistance stratum corneum and achieve sufficient electric fields in deeper tissues under low voltage without assistant of a microneedle-based electrode, we investigated RFP electroporation in skeletal muscle beneath the skin. As shown in Figure S6A, after the same preprocessing, we injected the plasmid into the muscle to address whether a strong-enough electric field was generated under the skin to achieve efficient electroporation. In Figure S6B, under the same electric pulse condition, the mouse thighs treated with

the microneedle roller expressed stronger fluorescence in a larger area, which indicated that the transfection rate was remarkably enhanced. Additionally, 50 V and 70 V pulses lead to better efficiency using our approach. Compared with the commercial plate electrode (Tweezertrodes, BTX, USA) with electroporation under 150 V, the electroporation under 50 V pulses by the proposed method showed

better performance. Taken together, with the assistance of a microneedle roller, a sufficient electric field could be generated in the tissue and the performance of FIEA was remarkably boosted. The comparison with a high-voltage commercial plate electrode process revealed that our minimally invasive method did reduce the electroporation voltage, and achieved high performance as well.

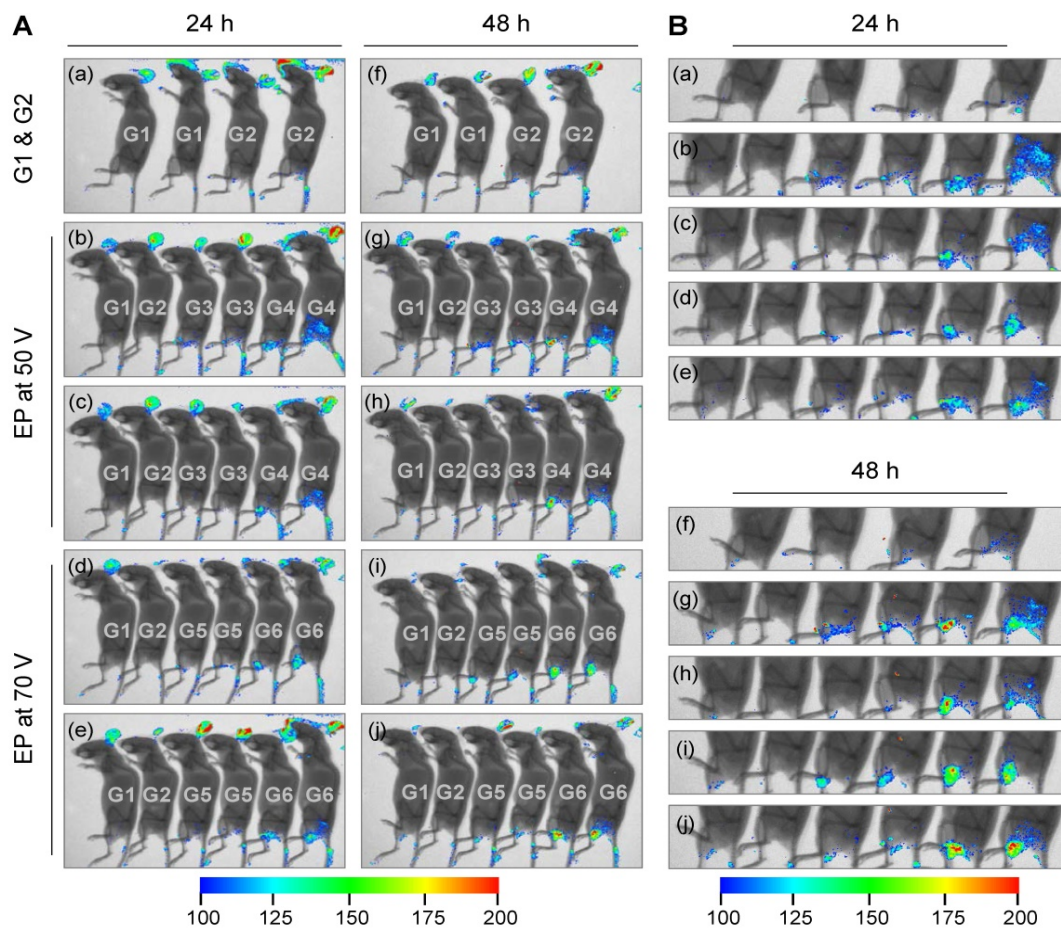
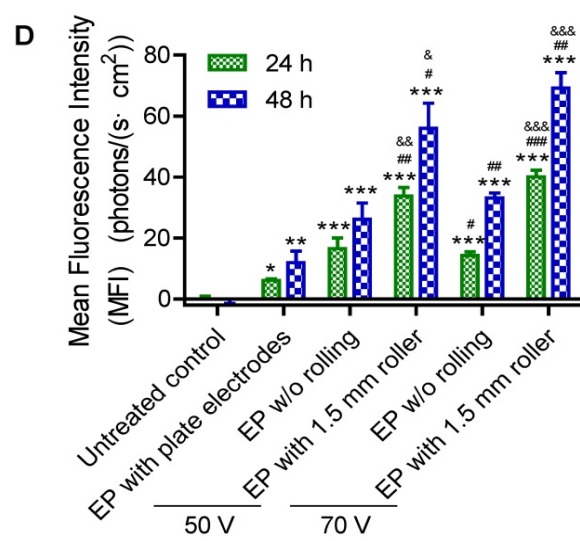


Figure 4. RFP electroporation in the skin. (A) The whole-body fluorescence intensity imaging indicates efficient RFP plasmid expression in electroporated mouse skin. Animals received the following treatments: (G1) without any treatment as negative control; (G2) electroporation with plate electrode at 100 V; (G3) electroporation with FIEA at 50 V without rolling; (G4) electroporation with FIEA at 50 V with rolling; (G5) electroporation with FIEA at 70 V without rolling; (G6) electroporation with FIEA at 70 V with rolling. Fluorescence images were merged with X-ray images to show the fluorescent sites. Electroporation conditions were: 10 electrical pulse; voltage 100, 50 or 70 V; 10 ms pulse duration; 1 s pulse interval. (B) Enlarged images from (A) indicating the electroporation areas of the mice. (C) Grouping information. (D) Quantitative analysis of (A) or (B). The mean fluorescence intensity (MFI) was calculated from 4 different mice. Data were normalized to an unelectroporated mouse who's MFI was set to zero. Each bar represents the mean \pm SEM. Statistical analyses were performed using two-tailed Student's t-test. *, vs. unelectroporated mice at the same time point, *P < 0.05, **P < 0.01, and ***P < 0.001. #, vs. mice electroporated with plate electrodes at the same time point, #P < 0.05, ##P < 0.01, and ###P < 0.001. &, vs. mice electroporated at the same voltage with FIEA but without rolling at the same time point, &P < 0.05, &&P < 0.01, and &&&P < 0.001.

- C**
- G1: Untreated control
 - G2: EP with plate electrodes at 100 V
 - G3: EP without rolling at 50 V
 - G4: EP with rolling at 50 V
 - G5: EP without rolling at 70 V
 - G6: EP with rolling at 70 V



Electroporation of Cy5-labelled siRNA in skin

RNA interference (RNAi) is recently regarded as a major tool that can revolutionize bioscience and biomedical fields [56]. It is crucial to develop appropriate approaches for short interfering RNA (siRNA) drug delivery to target issues *in vivo*, since it is difficult for the naked siRNA to cross cell membranes and is easily eliminated from the circulatory system [57-59]. As a localized delivery strategy, electroporation of siRNA to the skin has a large potential for clinical applications due to its high target specificity and lack of carrier, signifying no safety concerns unlike viral-based vectors.

We investigated the transdermal electroporation of Cy5-labelled siRNA using the technique established by us to assess the capability for transfecting siRNA to the skin. In a pilot study, a tissue cryosection was prepared and observed with a confocal microscope to visually evaluate if such a proposed method could deliver siRNA into the skin and how deep. Hence, a 0.5 mm long microneedle roller, the shortest roller we used in this study, was first employed in this assay. Confocal laser scanning microscopy (CLSM) images manifested that Cy5-labelled siRNA was dispersed in the whole full-thickness skin, as the white dotted line indicates (Figure 3B). The depth was $487 \pm 33 \mu\text{m}$, which is consistent with the simulation in Figure 2 showing that the electric field is larger than 400 V/cm (providing effective electroporation) below 500 μm .

In an additional full study, untreated mice were set as negative control (G2), while mice smeared with Cy5-labelled siRNA only (G1) were included as another control. All electroporation mice (G3-6) received ten pulses of stimulation at 70 V with 10 ms duration with different rolling conditions: G3, without rolling using the microneedle roller; G4, rolling with a 0.5 mm long microneedle roller; G5, rolling with a 1.0 mm long microneedle roller; and G6, rolling with a 1.5 mm long microneedle roller. The transfection performance was observed at 6 h and 24 h post treatment. As the whole-body fluorescence images in Figure 5A show, the delivery efficiency was obviously enhanced utilizing FIEA compared to the control groups, and the size of the region expressing fluorescence in these mice was superior than that of mice with siRNA painting alone. Furthermore, with strengthening of the penetration condition (from 0.5 mm long to 1.5 mm long microneedle roller), the MFI of siRNA in the skin increased. A longer microneedle could create a deeper conductive path within the skin, leading to an elevated electric field intensity beneath the skin (Figure S7) and strengthened permeation of drugs. Quantitative analysis of the data, as shown in

Figure 5B, manifested that a high level of siRNA delivery was achieved by the combined use of the microneedle roller and FIEA.

In order to further verify target specificity of our electroporation method, one mouse from each group was sacrificed at 6 h after electroporation by cervical dislocation, the target skins were isolated, and fluorescence image were acquired (Figure 5C). The correlation between transfection efficiency and experiment condition was similar to the data from whole-body imaging (Figure 5B). Moreover, the MFIs in isolated skins were almost numerically the same, hinting that the majority of the siRNA was transferred into the target skin. All of these data reveal that microchannels caused by the microneedle rollers could promote the electroporation capability. The proposed electroporation method could facilitate transdermal delivery of siRNA to skin, and enable high target specificity and satisfactory bioavailability of siRNA therapeutics.

Gene knockdown mediated by electroporated siRNA in skin

It is important to further verify if siRNA electroporated by the proposed method can mediate gene silencing *in vivo*. Therefore, siSCD1, an RNase-resistant siRNA targeting stearyl-CoA desaturase-1 (SCD1), was selected to perform this assay. SCD1 is a key enzyme involved in fatty acid metabolism. Elevated expression levels of SCD1 have been found to be correlated with obesity [60], tumor malignancy [61], and cardiac development [62]. Here, gene silencing efficiency was evaluated at both mRNA and protein levels. For the mRNA expression assay, five groups (six mice per group) of mice were given the following treatments: (1) electroporation at 70 V assisted by roller but without administration of siRNA, (2) smearing siRNA on the skin and rolled with the roller but without electroporation, (3) electroporation of siSCD1 without rolling, (4) electroporation of siSCD1 assisted by 0.5 mm long roller, (5) electroporation of siSCD1 assisted by 1.5 mm long roller. siRNA dosed at 10 μg per mouse (1 $\mu\text{g}/\mu\text{L}$, $\sim 0.5 \text{ mg/kg}$), and the in-life stage was terminated at 48 h post electroporation. Real-time PCR data revealed that SCD1's expression in the skin was significantly repressed in groups 4 and 5 as shown in Figure 6A, which were electroporated with FIEA at 70 V with pretreatment using 0.5 and 1.5 mm rollers, respectively. SCD1 expression in group 3, electroporation at 70 V without pre-rolling, was also inhibited to some extent. By contrast, two negative control groups of mice (groups 1 and 2) showed no gene knockdown in skin.

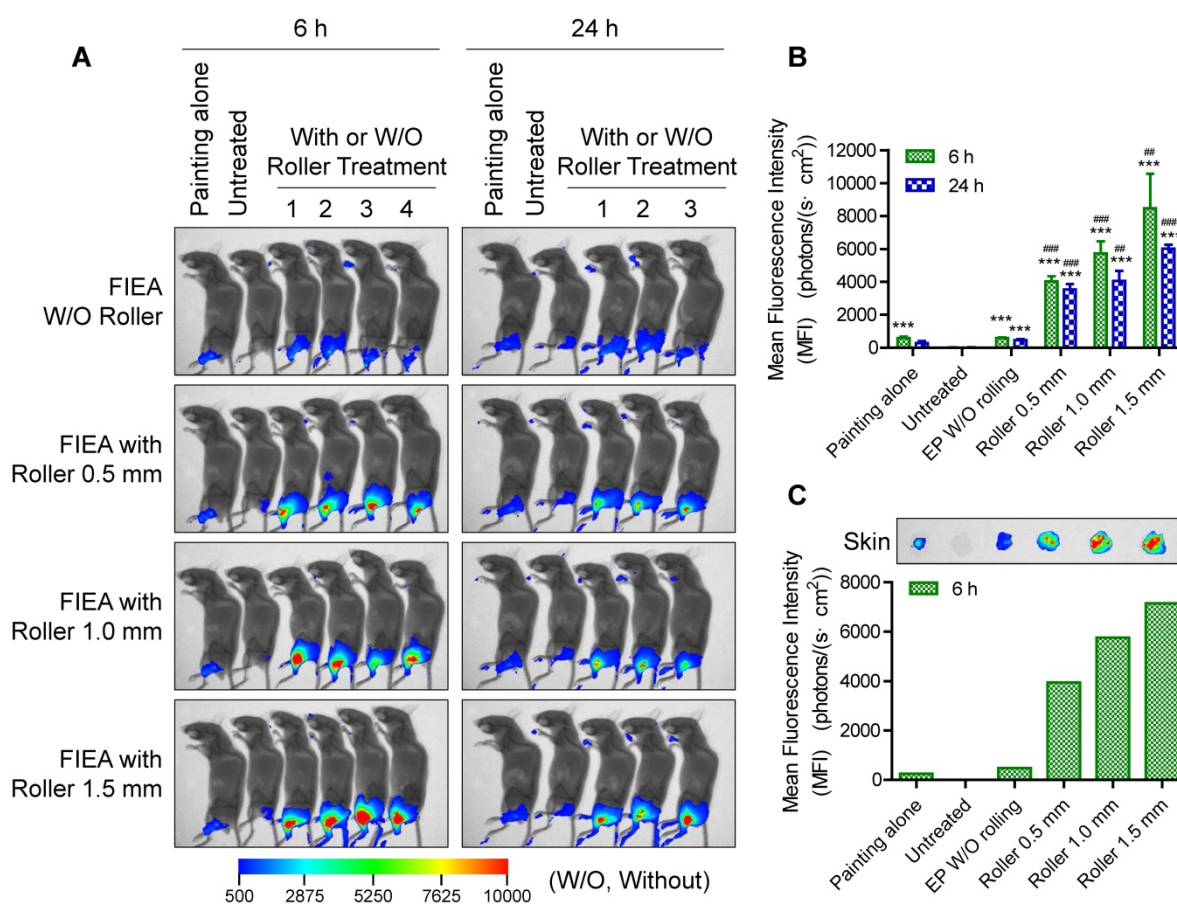


Figure 5. Fluorescence imaging of Cy5-labelled siRNA in mouse skin. (A) Whole-body fluorescence intensity imaging of electroporation of Cy5-siRNA in mouse skin. Animals received the following treatments: (G1) siRNA was directly painted on the skin but without further treatment; (G2) animals without any treatment as negative control; (G3) electroporation at 70 V without rolling; (G4-6) electroporation at 70 V facilitated by rolling with microneedle rollers with a length of 0.5, 1.0 or 1.5 mm. Fluorescence images were merged with X-ray images to show the fluorescence sites. Electroporation conditions were: 10 electrical pulse; voltage 70 V; 10 ms pulse duration; 1 s pulse interval. **(B)** Quantitative analysis of (A). The mean fluorescence intensity (MFI) was calculated from 4 (6 h) or 3 (24 h) different mice. Data were normalized to unelectroporated mice whose MFIs were set to zero. Each bar represents the mean \pm SEM. Statistical analyses were performed using two-tailed Student's t-test. *, vs. unelectroporated mice at the same time point, ***P < 0.001. #, vs. mice electroporated without rolling at the same time point, ###P < 0.01, and ###P < 0.001. **(C)** Fluorescence imaging of isolated skin at 6 h post treatment and the corresponding quantitative analysis result. One mouse was sacrificed for examination at 6 h post electroporation for each group of mice.

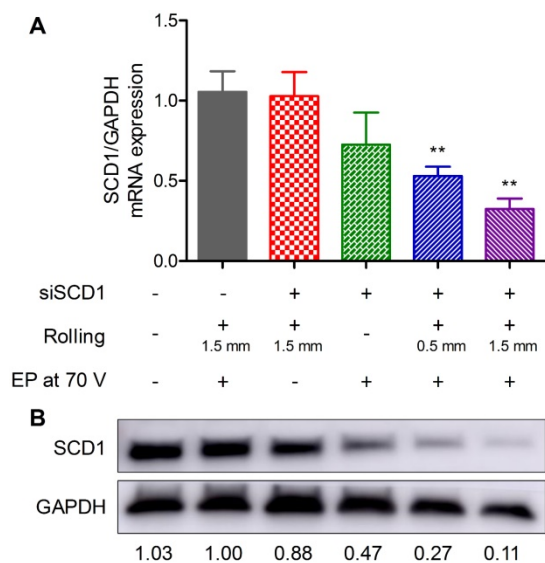


Figure 6. Gene silencing assay with anti-SCD1 siRNA (siSCD1). siRNA was electroporated under various conditions. mRNA (A) and protein (B) expression levels of SCD1 in skin. EP, electroporation. * vs. mice who received rolling and electroporation without administration of siRNA. **, P < 0.01.

For the protein expression assay, an additional group of mice without any treatment was also include as a negative control. Western blot was performed to analyze SCD1 protein expression in the skin. It was shown that the overall pattern was similar to the data from the mRNA expression assay (Figure 6B). The silencing efficiency was slightly different for mRNA, which might be attributed to the potential differences between mRNA and protein in their expression and degradation life course.

These data further demonstrated that siRNA electroporated with the proposed method mediated efficient gene silencing in the skin, and pre-penetration of the skin with a microneedle roller dramatically enhanced the permeability of the skin, and then elevated the electroporation efficiency.

Safety assessment of the suggested electroporation method

Safety is another important issue to assess when

considering if the proposed method can be clinically used to transfect nucleic acids into the skin. In the study of RFP electroporation, all animals were carefully monitored, and clinical observation was performed for two weeks post treatment. Clinical symptoms, including animal appearance, behavior, eating, drinking, response to stimulation, excretion, as well as skin appearance and muscle function at the electroporation position, were recorded during the whole process. It was shown that neither significant skin lesions nor functional impairment of muscles was observed. A slight burn was observed for those animals administered 70 V. The burn lines appeared in line with the electrodes, hinting that this might be caused by heating accompanying electroporation. However, these damages were completely recovered

within five days post treatment as shown in **Figure 7**. In addition, the proposed electroporation method barely caused damage to the muscle since no abnormal behavior or inconvenience in action was observed during the whole study course.

In mice (with the exception of albino strains), hair follicles and hairs contain a pigment produced by melanocytes, melanin. The morphology of the hair follicles changes with the follicle cycles, anagen (active growth, typically looks black), catagen (controlled regression through apoptosis, typically looks gray), and telogen (resting phase, typically looks white) [63]. At the beginning of hair depilation, the mice with gray and black skin on the legs were removed from this study, to avoid light absorption by the black materials. During the monitoring course,

hair growth cycle changes from telogen, to catagen, then to anagen, were observed as the skin color changed from white to gray, and to black. Along with this process, hair regrew on the skin, suggesting the normal function of the skin (**Figure 7**). Clinical observation was also performed in the study of siRNA electroporation, and similar phenomena were recorded during its course (**Figure S8**).

In addition to the observations at the macro level, we also performed a pathological analysis to thoroughly assess skin damage caused by the proposed electroporation method, which is an important consideration in pre-clinical studies of electroporation devices. Here, four groups of mice received the following treatments: (1) without any treatment; (2) rolled with a 1.5 mm long roller, but without electroporation; (3) electroporated at 70 V with FIEA, but without rolling; (4) rolled with the roller followed by electroporation at 70 V with FIEA. Tissue samples were collected at the indicated time points. Preparation of histopathologic sections and H&E staining were performed with standard protocols. In contrast to the untreated mice, significant lymphocytic infiltration was observed at the beginning (day 1 and 3) for all three groups of mice that suffered rolling, electroporation, or both, indicating inflammation occurred (**Figure 8**). The level of inflammation in group 4 was slight higher than that in groups 2 and 3, although no significant

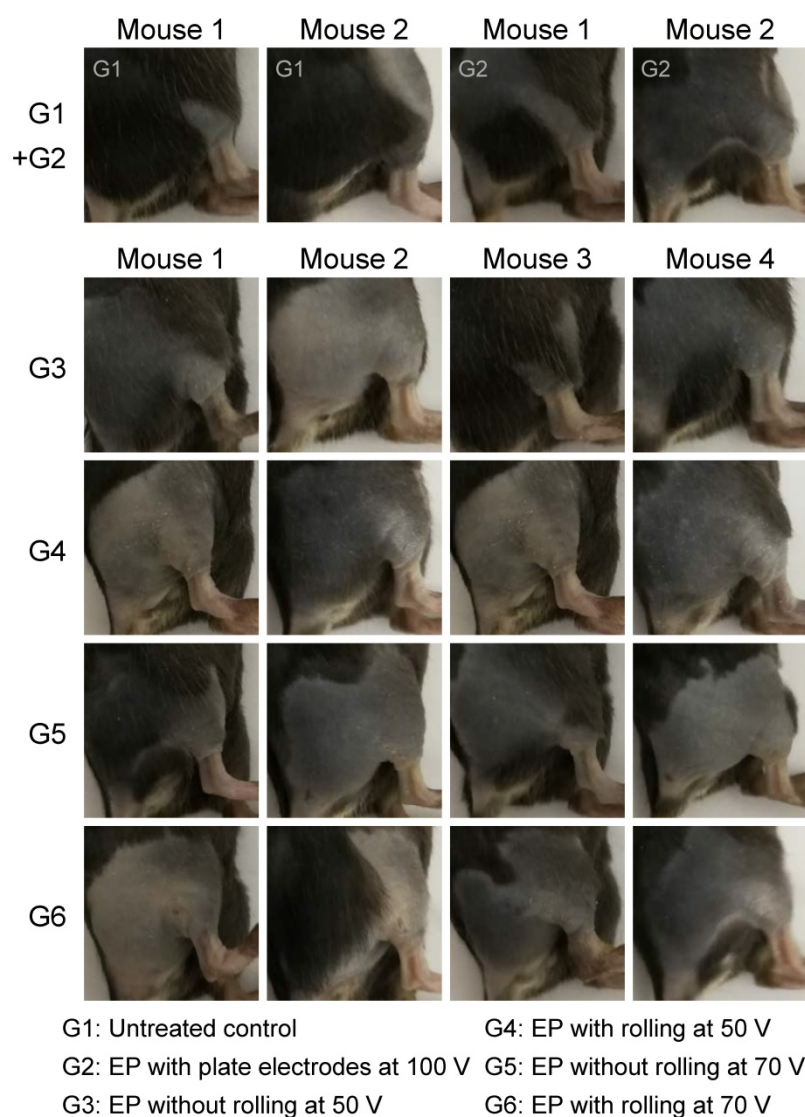


Figure 7. Mouse images acquired on day 5 after electroporation of RFP-expression plasmid. It was shown that the skin was healthy, the color of pre-depilated skin was gray or black, suggesting the hair growth cycle switched from telogen to catagen or anagen. Accordingly, some hair regrew on the skin.

difference was observed among these three groups. In addition, the inflammation was dramatically alleviated on day 6, and almost recovered on day 10. These observations are also in line with the clinical findings at the macro level.

Finally, we also investigated whether the drug entered the circulatory system. Cy5-labelled siRNA was used as an indicator in this assay and we used the proposed method to deliver the drug to the skin. Considering that the diffusion process of the drug entering the blood vessels might take a relatively long time, we collected blood samples from electroporated mice at different time points (5 min, 30 min, and 60 min). The blank blood acquired from untreated mice was included as a negative control, and a positive control was prepared by directly adding 5 μ g Cy5-labelled siRNA into another blank blood sample. Then all specimens were examined with an *in vivo* imaging system. Both imaging and quantitative analysis data revealed that no siRNA entered the circulatory system under the proposed experimental conditions (Figure S9).

Conclusions

Delivery of nucleic acid molecules into the skin remains a main barrier for gene-based therapy or

intradermal/subcutaneous vaccination. Here, we propose a novel electroporation method based on the combination use of a microneedle roller and a flexible interdigitated electroporation array (FIEA). By penetrating the skin with the microneedle roller, a conductive buffer played a role as liquid electrodes in the skin when electric pulses were applied. FIEA, benefitting from its flexible substrate and interdigitated electrodes, provided an even electric field both on the surface and inside the skin. As a result, successful gene (RFP) expression and siRNA transfection were achieved, and the performance of electroporation with the help of microneedle rolling was much superior to that without rolling. siRNA electroporation triggered significant gene silencing in the skin. Moreover, such an electroporation method exhibited no adverse effects to the skin and muscle of the treated mice, since a low voltage (50 V) was enough to accomplish this process and achieve efficient delivery. In summary, the combined use of a microneedle roller and FIEA showed ideal nucleic acid molecule transfection efficiency into mouse skin at a low voltage, which may support clinical application of such approach in the treatment of skin diseases or vaccination *via* the skin.

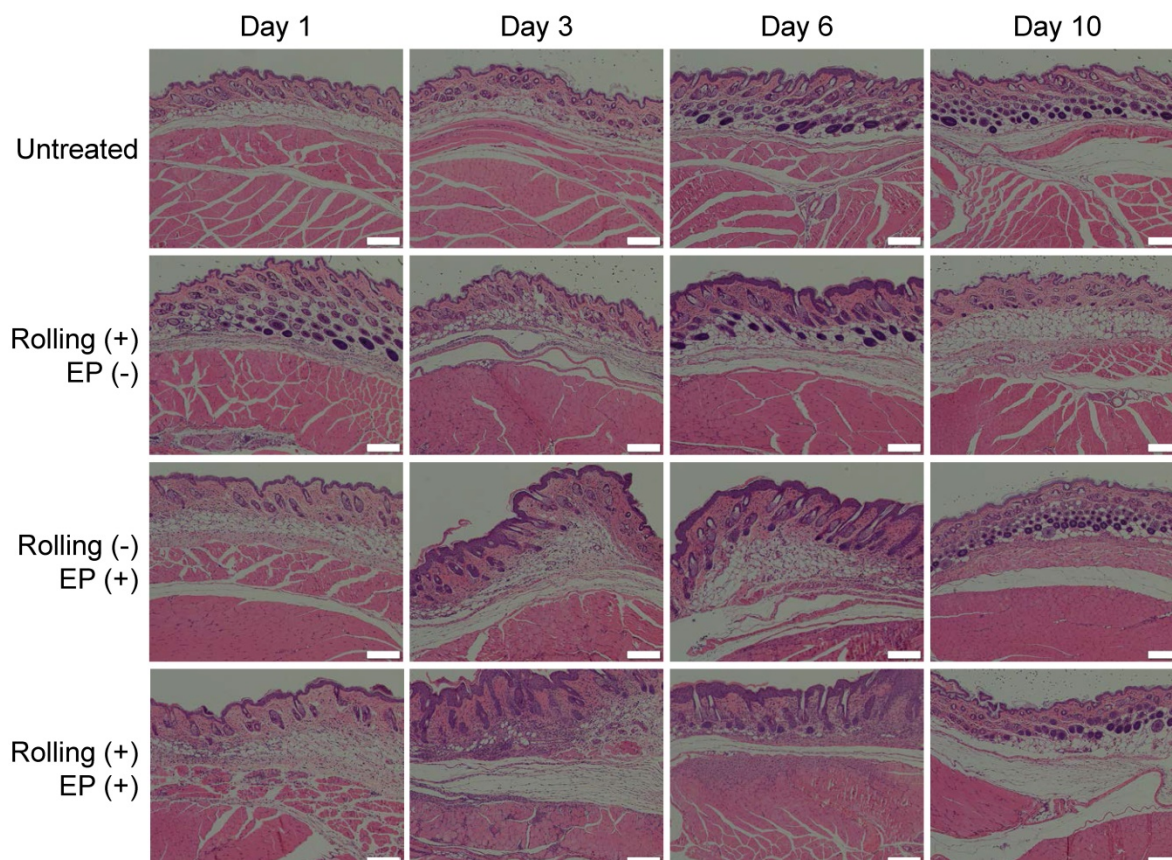


Figure 8. H&E staining of skin and muscle tissues that suffered various treatments. EP: electroporation. Scale bar, 200 μ m.

Abbreviations

EP: electroporation; FIEA: flexible interdigitated electroporation array; MEMS: micro-electromechanical system; SPF: specific pathogen free; SCD1: stearyl-CoA desaturase-1; OCT: optimal cutting temperature; NIR: near-infrared; DAPI: 4',6-diamidino-2-phenylindole; MFI: mean fluorescence intensity; CLSM: confocal laser scanning microscopy.

Acknowledgement

This work was supported by the National Key Research and Development Program of China (No. 2016YFA0200802), the National Natural Science Foundation of China (91323304, 81402863, 81402863), and the funding from Beijing Institute of Technology (to Y. H.).

Author contributions

Y. H., Zh. L., D. H. and D. Z. designed the research. Y. H. led the research. D. H., and Z. W. fabricated the device and performed the COMSOL simulation. Y. H., D. Z. D. H., C. L., and T. Y. performed the animal assays. D. H., D. Z., Y. H., L. D., Z. W., X. W., Q. C., H. C. and Z. L. analyzed the data and provided helpful discussion. D. H., Y. H. and D. Z. wrote the manuscript. All authors discussed the results and commented on the paper.

Supplementary Material

Supplementary figures and tables.

<http://www.thno.org/v08p2361s1.pdf>

Competing Interests

The authors have declared that no competing interest exists.

References

1. Thomas CE, Ehrhardt A, Kay MA. Progress and problems with the use of viral vectors for gene therapy. *Nat Rev Genet.* 2003; 4: 346-58.
2. Lollini PL, Cavallo F, Nanni P, Forni G. Vaccines for tumour prevention. *Nat Rev Cancer.* 2006; 6: 204-16.
3. Xu H, Li Z, Si J. Nanocarriers in Gene Therapy: A Review. *J Biomed Nanotechnol.* 2014; 10: 3483-507.
4. Gotherf A, Mahmood F, Dagnaes-Hansen F, Gehl J. Efficacy of transgene expression in porcine skin as a function of electrode choice. *Bioelectrochemistry.* 2011; 82: 95-102.
5. Roos A-K, Moreno S, Leder C, Pavlenko M, King A, Pisa P. Enhancement of cellular immune response to a prostate cancer DNA vaccine by intradermal electroporation. *Mol Ther.* 2006; 13: 320-7.
6. Hirao LA, Wu L, Khan AS, Satishchandran A, Draghia-Akli R, Weiner DB. Intradermal/subcutaneous immunization by electroporation improves plasmid vaccine delivery and potency in pigs and rhesus macaques. *Vaccine.* 2008; 26: 440-8.
7. Medi BM, Layek B, Singh J. Electroporation for Dermal and Transdermal Drug Delivery. In: Dragicevic N, I. Maibach H, editors. *Percutaneous Penetration Enhancers Physical Methods in Penetration Enhancement.* Berlin, Heidelberg: Springer Berlin Heidelberg; 2017. p. 105-22.
8. Regnier V, De Morre N, Jadoul A, Pr at V. Mechanisms of a phosphorothioate oligonucleotide delivery by skin electroporation. *Int J Pharm.* 1999; 184: 147-56.
9. Cevc G. Transfersomes, liposomes and other lipid suspensions on the skin: permeation enhancement, vesicle penetration, and transdermal drug delivery. *Crit Rev Ther Drug Carrier Syst.* 1996; 13: 257-388.

10. Williams AC, Barry BW. Penetration enhancers. *Adv Drug Deliv Rev.* 2012; 64: 128-37.
11. Du L, Zhou J, Meng L, Wang X, Wang C, Huang Y, et al. The pH-Triggered Triblock Nanocarrier Enabled Highly Efficient siRNA Delivery for Cancer Therapy. *Theranostics.* 2017; 7: 3432-45.
12. Liao AH, Lu YJ, Lin YC, Chen HK, Sytwu HK, Wang CH. Effectiveness of a Layer-by-Layer Microbubbles-Based Delivery System for Applying Minoxidil to Enhance Hair Growth. *Theranostics.* 2016; 6: 817-27.
13. Zhou J, Wu Y, Wang C, Cheng Q, Han S, Wang X, et al. pH-Sensitive Nanomicelles for High-Efficiency siRNA Delivery *in vitro* and *in vivo*: An Insight into the Design of Polycations with Robust Cytosolic Release. *Nano Lett.* 2016; 16: 6916-23.
14. Escobar-Chavez JJ, Merino V, Lopez-Cervantes M, Rodriguez-Cruz IM, Quintanar-Guerrero D, Ganem-Quintanar A. The Use of Iontophoresis in the Administration of Nicotine and New Non-Nicotine Drugs through the Skin for Smoking Cessation. *Curr Drug Discov Technol.* 2009; 6: 171-85.
15. Newman CM, Bettinger T. Gene therapy progress and prospects: ultrasound for gene transfer. *Gene Ther.* 2007; 14: 465-75.
16. Donate A, Coppola D, Cruz Y, Heller R. Evaluation of a novel non-penetrating electrode for use in DNA vaccination. *PLoS One.* 2011; 6: e19181.
17. Brave A, Gudmundsdottir L, Sandstrom E, Haller BK, Hallengard D, Maltais AK, et al. Biodistribution persistence and lack of integration of a multigene HIV vaccine delivered by needle-free intradermal injection and electroporation. *Vaccine.* 2010; 28: 8203-9.
18. Hirao LA, Draghia-Akli R, Prigge JT, Yang M, Satishchandran A, Wu L, et al. Multivalent smallpox DNA vaccine delivered by intradermal electroporation drives protective immunity in nonhuman primates against lethal monkeypox challenge. *J Infect Dis.* 2011; 203: 95-102.
19. Gotherf A, Hojman P, Gehl J. Therapeutic levels of erythropoietin (EPO) achieved after gene electrotransfer to skin in mice. *Gene Ther.* 2010; 17: 1077-84.
20. Ferraro B, Cruz YL, Coppola D, Heller R. Intradermal Delivery of Plasmid VEGF(165) by Electroporation Promotes Wound Healing. *Mol Ther.* 2009; 17: 651-7.
21. Wong T-W, Chen T-Y, Huang C-C, Tsai J-C, Hui SW. Painless Skin Electroporation as a Novel Way for Insulin Delivery. *Diabetes Technol Ther.* 2011; 13: 929-35.
22. Marrero B, Shirley S, Heller R. Delivery of Interleukin-15 to B16 Melanoma by Electroporation Leads to Tumor Regression and Long-term Survival. *Technol Cancer Res Treat.* 2014; 13: 551-60.
23. Ugen KE, Kutzler MA, Marrero B, Westover J, Coppola D, Weiner DB, et al. Regression of subcutaneous B16 melanoma tumors after intratumoral delivery of an IL-15-expressing plasmid followed by *in vivo* electroporation. *Cancer Gene Ther.* 2006; 13: 969-74.
24. Juan Escobar-Chavez J, Bonilla-Martinez D, Angelica Villegas-Gonzalez M, Luisa Revilla-Vazquez A. Electroporation as an Efficient Physical Enhancer for Skin Drug Delivery. *J Clin Pharmacol.* 2009; 49: 1262-83.
25. Li J, Liu F, Gupta S, Li C. Interventional Nanotheranostics of Pancreatic Ductal Adenocarcinoma. *Theranostics.* 2016; 6: 1393-402.
26. Gotherf A, Gehl J. Gene Electrotransfer to Skin; Review of Existing Literature and Clinical Perspectives. *Curr Gene Ther.* 2010; 10: 287-99.
27. Heller LC, Jaroszeski MJ, Coppola D, McCray AN, Hickey J, Heller R. Optimization of cutaneous electrically mediated plasmid DNA delivery using novel electrode. *Gene Ther.* 2006; 14: 275-80.
28. Maz eres S, Sel D, Golzio M, Pucihar G, Tamzali Y, Miklavcic D, et al. Non invasive contact electrodes for *in vivo* localized cutaneous electropulsation and associated drug and nucleic acid delivery. *J Control Release.* 2009; 134: 125-31.
29. Aihara H, Miyazaki J. Gene transfer into muscle by electroporation *in vivo*. *Nat Biotechnol.* 1998; 16: 867-70.
30. Staal LG, Gilbert R. Generators and Applicators: Equipment for Electroporation. In: Kee ST, Gehl J, Lee EW, editors. *Clinical Aspects of Electroporation.* New York, NY: Springer New York; 2011. p. 45-65.
31. Prausnitz MR, Langer R. Transdermal drug delivery. *Nat Biotechnol.* 2008; 26: 1261-8.
32. Hofmann GA. Instrumentation and electrodes for *in vivo* electroporation. *Electrochemotherapy, Electrotherapy, and Transdermal Drug Delivery.* 2000; 37: 37-61.
33. Wei Z, Zheng S, Wang R, Bu X, Ma H, Wu Y, et al. A flexible microneedle array as low-voltage electroporation electrodes for *in vivo* DNA and siRNA delivery. *Lab Chip.* 2014; 14: 4093-102.
34. Sajjilafu, Hur E-M, Zhou F-Q. Genetic dissection of axon regeneration via *in vivo* electroporation of adult mouse sensory neurons. *Nat Commun.* 2011; 2: 543.
35. Choi SO, Kim YC, Park JH, Hutcheson J, Gill HS, Yoon YK, et al. An electrically active microneedle array for electroporation. *Biomed Microdevices.* 2010; 12: 263-73.
36. Choi S-O, Kim Y-C, Lee JW, Park J-H, Prausnitz MR, Allen MG. Intracellular Protein Delivery and Gene Transfection by Electroporation Using a Microneedle Electrode Array. *Small.* 2012; 8: 1081-91.
37. Donnelly RF, Singh TRR, Garland MJ, Migalska K, Majithiya R, McCrudden CM, et al. Hydrogel-Forming Microneedle Arrays for Enhanced Transdermal Drug Delivery. *Adv Funct Mater.* 2012; 22: 4879-90.
38. Lee JW, Choi S-O, Felner EI, Prausnitz MR. Dissolving Microneedle Patch for Transdermal Delivery of Human Growth Hormone. *Small.* 2011; 7: 531-9.

39. Wu M, Zhao D, Zhong W, Yan H, Wang X, Liang Z, et al. High-density distributed electrode network, a multi-functional electroporation method for delivery of molecules of different sizes. *Sci Rep.* 2013; 3: 3370.
40. Zhao D, Huang D, Li Y, Wu M, Zhong W, Cheng Q, et al. A Flow-Through Cell Electroporation Device for Rapidly and Efficiently Transfecting Massive Amounts of Cells *in vitro* and *ex vivo*. *Sci Rep.* 2016; 6: 18469.
41. Gill HS, Soderholm J, Prausnitz MR, Sallberg M. Cutaneous vaccination using microneedles coated with hepatitis C DNA vaccine. *Gene Ther.* 2010; 17: 811-4.
42. Pinyon JL, Tadros SF, Froud KE, et al. Close-Field Electroporation Gene Delivery Using the Cochlear Implant Electrode Array Enhances the Bionic Ear. *Sci Transl Med.* 2014; 6: 233ra54-ra54.
43. Pamornpathomkul B, Wongkajornsilp A, Laiwattanapaisal W, Rojanarata T, Opanasopit P, Ngawhirunpat T. A combined approach of hollow microneedles and nanocarriers for skin immunization with plasmid DNA encoding ovalbumin. *Int J Nanomedicine.* 2017; 12: 885-98.
44. Wei Z, Huang Y, Zhao D, Hu Z, Li Z, Liang Z. A Pliable Electroporation Patch (ep-Patch) for Efficient Delivery of Nucleic Acid Molecules into Animal Tissues with Irregular Surface Shapes. *Sci Rep.* 2015; 5: 7618.
45. Huang D, Zhao D, Li J, Du L, Wei Z, Liang Z, et al. A minimally invasive *in vivo* electroporation method utilizing flexible electrode and microneedle roller. 19th International Conference on Solid-State Sensors, Actuators and Microsystems; 2017 Jun 18 - Jun 22; Kaohsiung, Taiwan. New York: IEEE; 2017. p. 1684-1687.
46. Yu J, Zhang Y, Ye Y, DiSanto R, Sun W, Ranson D, et al. Microneedle-array patches loaded with hypoxia-sensitive vesicles provide fast glucose-responsive insulin delivery. *Proc Natl Acad Sci U S A.* 2015; 112: 8260-5.
47. Zhang Y, Liu Q, Yu J, Yu S, Wang J, Qiang L, et al. Locally Induced Adipose Tissue Browning by Microneedle Patch for Obesity Treatment. *ACS Nano.* 2017; 11: 9223-30.
48. Zhang Y, Yu J, Wang J, Hanne NJ, Cui Z, Qian C, et al. Thrombin-Responsive Transcutaneous Patch for Auto-Anticoagulant Regulation. *Adv Mater.* 2017; 29. DOI: 10.1002/adma.201604043
49. Ye Y, Wang C, Zhang X, Hu Q, Zhang Y, Liu Q, et al. A melanin-mediated cancer immunotherapy patch. *Sci Immunol.* 2017; 2. DOI: 10.1126/sciimmunol.aan5692.
50. Gabriel C, Peyman A, Grant EH. Electrical conductivity of tissue at frequencies below 1 MHz. *Phys Med Biol.* 2009; 54: 4863-78.
51. [Internet] Center for Drug Evaluation. Beijing: China Food and Drug Administration; [update 2014 may 13; cited 2017 Oct 22]. Available from: <http://www.cde.org.cn/zdyz.do?method=largePage&id=189>. Chinese.
52. Badran MM, Kuntsche J, Fahr A. Skin penetration enhancement by a microneedle device (Dermaroller®) *in vitro*: Dependency on needle size and applied formulation. *European Journal of Pharmaceutical Sciences.* 2009; 36: 511-23.
53. Khavari PA. Gene therapy for genetic skin disease. *J Invest Dermatol.* 1998; 110: 462-7.
54. Bracke S, Carretero M, Guerrero-Aspizua S, Desmet E, Illera N, Navarro M, et al. Targeted silencing of DEFB4 in a bioengineered skin-humanized mouse model for psoriasis: development of siRNA SECosome-based novel therapies. *Exp Dermatol.* 2014; 23: 199-201.
55. Ntziachristos V, Bremer C, Weissleder R. Fluorescence imaging with near-infrared light: new technological advances that enable *in vivo* molecular imaging. *Eur Radiol.* 2003; 13: 195-208.
56. Bobbin ML, Rossi JJ. RNA Interference (RNAi)-Based Therapeutics: Delivering on the Promise? *Annu Rev Pharmacol Toxicol.* 2016; 56: 103-22.
57. Draz MS, Fang BA, Zhang P, Hu Z, Gu S, Weng KC, et al. Nanoparticle-mediated systemic delivery of siRNA for treatment of cancers and viral infections. *Theranostics.* 2014; 4: 872-92.
58. Huang Y, Hong J, Zheng S, Ding Y, Guo S, Zhang H, et al. Elimination pathways of systemically delivered siRNA. *Mol Ther.* 2011; 19: 381-5.
59. Huang Y, Cheng Q, Ji JL, Zheng S, Du L, Meng L, et al. Pharmacokinetic Behaviors of Intravenously Administered siRNA in Glandular Tissues. *Theranostics.* 2016; 6: 1528-41.
60. Flowers MT, Ntambi JM. Role of stearoyl-coenzyme A desaturase in regulating lipid metabolism. *Curr Opin Lipidol.* 2008; 19: 248-56.
61. Mohammadzadeh F, Mosayebi G, Montazeri V, Darabi M, Fayezi S, Shaaker M, et al. Fatty Acid Composition of Tissue Cultured Breast Carcinoma and the Effect of Stearoyl-CoA Desaturase 1 Inhibition. *J Breast Cancer.* 2014; 17: 136-42.
62. Zhang L, Pan Y, Qin G, Chen L, Chatterjee TK, Weintraub NL, et al. Inhibition of stearoyl-coA desaturase selectively eliminates tumorigenic Nanog-positive cells: improving the safety of iPS cell transplantation to myocardium. *Cell Cycle.* 2014; 13: 762-71.
63. Muller-Rover S, Handjiski B, van der Veen C, Eichmuller S, Foitzik K, McKay IA, et al. A comprehensive guide for the accurate classification of murine hair follicles in distinct hair cycle stages. *J Invest Dermatol.* 2001; 117: 3-15.